Showcasing research on low-temperature solid oxide solutions as catalyst supports from Ewa Iwanek's laboratory, Faculty of Chemistry, Warsaw University of Technology, Warsaw, Poland.

Boosting the activity of silver catalysts for soot combustion by modification of the alumina support

The colorful doped-alumina supports serve as a backdrop and the active phase, metallic silver, reigns over the whole process. The three gears which work together for enhanced activity in soot combustion are: choice of (1) host oxide, (2) dopant and (3) their ratio. The artwork was prepared by Paulina Halina Marek-Urban.

Image reproduced by permission of Ewa M. Iwanek from *J. Mater. Chem. A,* 2025, **13**, 41764.

As featured in:

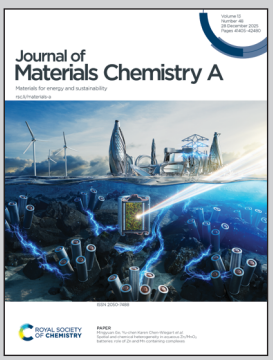

See Ewa M. Iwanek (nee Wilczkowska) *et al.,* *J. Mater. Chem. A,* 2025, **13**, 41764.

ROYAL SOCIETY OF CHEMISTRY

rsc.li/materials-a

Registered charity number: 207890

Journal of Materials Chemistry A

ROYAL SOCIETY OF CHEMISTRY

PAPER

View Article Online
View Journal | View Issue

Cite this: J. Mater. Chem. A, 2025, 13, 41764

Boosting the activity of silver catalysts for soot combustion by modification of the alumina support

Ewa M. Iwanek (nee Wilczkowska), * Aleksandra Goździk, Piotr Winiarek, Paweł Falkowski, Maciej Dębowski and Wojciech Patkowski

Catalysts with 15 wt% Ag supported on alumina and alumina-based solid solutions were synthesized and characterized using a variety of techniques such as SEM-EDX, XRD, N_2-physisorption, TPR, CO_2-TPD, FTIR, ToF-SIMS and Hammett indicator tests. Their activity in tight-contact soot combustion was evaluated. The aim of the studies was to determine how the surface and structure of the support influence the activity of the supported Ag catalysts. A series of alumina supports calcined at temperatures ranging between 550 °C and 1300 °C were obtained and used as supports for silver to investigate the Ag-support interactions. XRD studies revealed that the supports calcined below 1000 °C contain low-temperature alumina polymorphs, but those calcined at or above this temperature contain α-alumina. Catalysts supported on α-alumina were more active. ToF-SIMS measurement results indicate that this step-wise change can be attributed to differences in the surface of the undoped alumina and Hammett indicator tests revealed that the acidic sites in supports calcined above 1000 °C require lower regeneration temperatures. The modification of the alumina support with ions such as cobalt, cerium and chromium ions prior to silver deposition can improve catalytic activity in soot oxidation. The catalysts with doped-alumina supports exhibit a similar activity and surfaces properties, including acidity, to Ag/α-alumina catalysts. These studies show that the same effect can obtained by two different methods, one of them being doping the support.

Received 24th July 2025
Accepted 17th October 2025

DOI: 10.1039/d5ta05994a

rsc.li/materials-a

1 Introduction

The most common supports for silver catalysts are alumina, ceria and zirconia.[1–6] Therefore, much is known about silver supported on specific pure oxides. There is some dispute about the catalytic form of silver, *i.e.* Ag^0/Ag^+, though in the case of alumina most studies affirm the presence of the metallic form of silver in the XRD patterns.[1,5,7–9] Nevertheless, the findings of experiments employing techniques such as temperature-programmed-reduction also demonstrate the presence of oxidized silver species on the surface.[10–12] The same is true for oxygen species: different types of oxygen ions have been detected on the surface of silver catalysts.[8,13,14] Research indicates that there is a dependence of the Ag loading on the type and relative abundance of oxygen species on the surface of the catalyst. Hence, in this study a fixed silver loading was used to focus on the support influence. Due to the fact that different oxygen and silver species can be expected on the surface of the catalysts, a technique called Time-of-Flight Secondary Ion Mass Spectrometry was implemented to probe the relative ease of extraction of secondary ions from the surface of the oxide. Considering the excellent surface spatial resolution of the technique, it is much underused in catalysis where it could be a great asset.[15–19] However, this is due to the numerous variables which contribute to the complex mass spectrum and difficulties in interpretation of results. When comparing different oxides, *e.g.* SiO_2 and Al_2O_3, the comparison might not be very meaningful because there are too many parameters which differ between the two samples: the nature of Si^{4+} and Al^{3+} themselves, the coordination of the cation, bond lengths, *etc.* However, in the case of this study, the comparisons are made between samples of an oxide with the same cation of the same valency (Al^{3+}) obtained from the same precursor, differing only in the support calcination temperature. Hence, the ease of extraction of specific ions can be meaningfully compared between these supports. Our recently published paper showed that ToF-SIMS studies might hold a key to understanding how differences in the silver–alumina interactions can impact the catalytic activity of these systems in soot combustion,[20] prompting us to perform further studies with a series of alumina supports calcined at different temperatures. The "matrix effect", which is typically viewed as a flaw of the technique[21–23] because it yields different relative intensities of secondary ions depending on the chemical environment of species on the surface of the sample and is an advantage when investigating the effect of support calcination temperature on its interaction with silver.

Faculty of Chemistry, Warsaw University of Technology, Noakowskiego 3, 00-664 Warsaw, Poland. E-mail: ewa.iwanek@pw.edu.pl

The challenge in studying low-temperature alumina polymorphs as catalytic supports consists of two primary issues: the diffraction pattern of low-temperature polymorphs often yields only a few broad peaks in the diffraction pattern[1,5,9,20,24,25] and secondly that the alumina support can react with the active metal, *e.g.* nickel, to form a spinel such as $NiAl_2O_4$ as shown by Alreshaidan *et al.*[26] showed for alumina supported catalysts. Our recently published paper also indicated that with A, X and Y zeolites the relative abundance of metallic *vs.* bound silver depends on the type of zeolite.[20] We found that a part of the silver reacts with the zeolite surface leading to pronounced changes in the relative peak height ratios in the diffraction pattern of the original zeolite and some forms metallic silver particles on top of the support. Such observations have been also made by Ruan *et al.* with Ag/HZSM-5 catalysts which contain two types of silver on the surface: apart from metallic silver, Z–O–Ag clusters have also been found on the surface.[27] The latter were found, as in our studies, to be highly stable and hence the formation of Z–O–Ag moieties on zeolites[28,29] prevented silver from agglomerating even upon heating to 800 °C. In contrast to changes in the relative peak height ratios in the diffraction patterns of zeolites, changes in low-temperature alumina polymorphs would be difficult to monitor, as the diffraction patterns do not have well-defined sharp peaks[1,5,9,14,20] and any impact of the incorporation of foreign ions into the support might not be visible. In contrast, by heating the supports to 1300 °C to obtain α-alumina, intensive peaks are expected. In the present paper, three different ions, namely cerium, cobalt and chromium, were incorporated into a low-temperature alumina polymorph, synthesized at 550 °C.

A portion of the prepared alumina solid solution was further treated to 1300 °C. Cobalt is known to form a spinel with alumina, the so-called "cobalt blue", which is used as a pigment in ceramics.[30–33] A comprehensive study on the synthesis conditions of $CoAl_2O_4$ has revealed that the preparation of this spinel often comes with either Co_2AlO_4 or Co_3O_4. These phases differ in that though both have Co^{2+} ions in tetrahedral sites, per one Co^{2+} ion, Co_2AlO_4 has one and Co_3O_4 has two Co^{3+} ions in octahedral sites.[33] Solid solutions with chromium incorporated into the alumina lattice have been studied in terms of their optical, structural and mechanical properties.[34–36] These studies have shown that the amount of chromium incorporated into the alumina determines the volume of the unit cell due to the discrepancy of the ionic radii, namely 0.675 Å for Al^{3+} and 0.775 Å for Cr^{3+}. The solid solution of Ce-doped alumina[37–40] has also been studied to determine the influence of cerium ions on the aforementioned properties, but rarely applied in catalysis. A paper by Perez-Pastenes *et al.* implemented ^{27}Al NMR spectroscopy, which suggested that the presence of cerium ion in the alumina lattice slightly changed the coordination of Al^{3+} ions in comparison to that in undoped alumina.[38] In a Pt–Sn propane dehydrogenation catalyst supported on cerium-doped mesoporous alumina, it was observed that cerium ions "modify the acid function of the catalysts" as well impact the metallic phases themselves.[40] This is interesting and worth investigating in other catalytic systems for other reactions, such as silver catalysts for soot combustion and was one of the reasons for selecting cerium as one of the dopants.

In various catalytic reactions, the importance of the acidity of the support is emphasized.[8,41–43] In reference to selective catalytic reduction of NO with methane it has been stated that: "The acidity of these supports was considered key to stabilizing the active state of the metal species".[8] There are several methods which can be used to probe the acidic and basic sites of a catalytic support as well as probing oxygen vacancies and active oxygen species, including temperature programmed desorption of compounds such as NH_3,[44–46] O_2 (ref. 47–49) and CO_2,[25,50,51] electron paramagnetic resonance spectroscopy[52–54] and Hammett indicator tests.[55–58] All of these have advantages and disadvantages. The most substantial disadvantage of Hammett indicator tests is that they involve the assessment of color changes which can be obscured in the case of supports which are colored, but they are very accurate in the measuring the strength of both acidic and basic sites on the tested support. In the current study all of the undoped alumina samples were white regardless of their calcination temperature and were tested with Hammett indicators. The method was also tried on the prepared solid solution supports.

2 Results and discussion

2.1 Undoped alumina supports

The results of our recently published study revealed the superior activity of a silver catalyst supported on α-alumina with a low-surface area, high-temperature alumina polymorph, compared to that supported on a high-surface area, low-temperature polymorph.[20] These results prompted us to synthesize a series of alumina-supported catalysts calcined within the temperature range 550–1300 °C. The maximum soot combustion temperatures noted for these systems in activity measurements can be seen in Fig. 1A. The silver catalysts produced on the support calcined at 550 °C, Ag/Al-550, exhibits the maximum soot combustion rate at 574 °C (Fig. 1A solid vertical line). This temperature is higher for the alumina calcined at 700 °C, Ag/Al-700, and even higher for the catalyst supported on alumina calcined at 900 °C, Ag/Al-900 (Fig. 1A dashed-and-dotted line). A gradual decrease of the activity with an increase in the support calcination temperature due to the decrease in surface area (Fig. 1B), is expected. However, with further increase of the support calcination temperature the trend stops and a step-wise increase in the activity is observed (Fig. 1A). There was a substantial drop in the surface area (from 114 to 40.4 $m^2\ g^{-1}$) but this only caused an increase of T_{max} by approximately 11°, hence the decrease of T_{max} to 537 °C observed after support calcination at 1000 °C is significant. The calcination of alumina at even higher temperatures leads to a slight decrease in the activity of the silver catalyst, which again corresponded with a slight decrease of the surface area (Fig. 1B).

The catalysts themselves were also tested without soot in accordance with the same temperature program as the soot combustion tests to verify that the calcination procedure ensures that any changes of the catalysts do not lead to misinterpretation of the catalytic results. The silver supported on

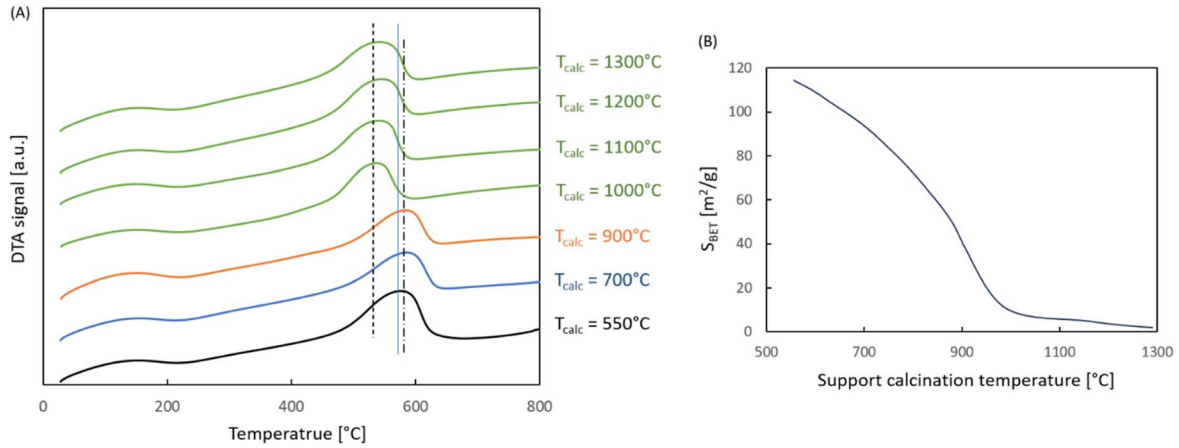

Fig. 1 Catalyst properties: (A) soot combustion activity results of Ag/alumina samples; initial alumina calcination temperature is indicated on the right; solid line: T_{max} with Ag/Al-550, dashed-and-dot line: highest T_{max} with Ag/Al-900, and dashed line: lowest T_{max} with Ag/Al-1000, and (B) surface area results.

alumina catalysts did not exhibit any noticeable changes in the mass loss curves regardless of the support calcination temperature. The curves obtained for Ag/Al-550 and Ag/Al-1300 are depicted in Fig. S1A and B, respectively revealing no substantial changes. However, it can be seen in the comparison of backscattered electron images of the fresh and spent Ag/Al-550 (SI, Fig. S2A and B, respectively) that the silver particles change their shape and size (increased particle) during the activity measurement.

Moreover, cyclic activity tests soot combustion tests, such as in ref. 59 and 60 were performed in order to further investigate this reaction. The cyclic tests were performed in order to verify if the results are reproducible. The results of the cyclic tests of Ag/Al-1300 show that there is no suppression of the activity of this catalyst in six consecutive cycles (SI, Fig. S3A). However, the backscattered images of the fresh Ag/Al-1300 and that used in 6 cycles (Fig. S2C and D, respectively) indicate a substantial growth of silver particles. The silver particles have significantly enlarged as a result of the cycling, which led to a reduced uptake of ammonia in NH_3-TPD studies from 0.145 to 0.129 $cm^3\ g^{-1}$. The values are very low, but considering the high calcination temperature, *i.e.* 1300 °C, large uptake quantities were not expected.

Isothermal soot combustion tests were performed to allow more time at temperatures at which soot combustion already occurs. Two types of isothermal soot combustion tests were performed, both starting at 420 °C: one with 3 h-long isothermal segments, Iso1, and the other with 6 h-long isothermal segments, Iso2 (for more details see Experimental section). The results obtained for Ag/Al-1300 (black curve) and the support itself (Al-1300, orange curve) run in Program 1 (Iso1) are compiled in Fig. S4A. The experiments show that the soot mixed with the catalyst combusts practically until completion (exponentially) in the first three hours of the experiment, whereas in the case of the support itself, the reaction is much slower and appears to have different rate slopes likely induced by the slight step increases in temperature that it is the small temperature steps that initiate a rate of reaction change. A very similar mass loss curve was observed for soot (Fig. S4B, green curve), which shows that Al-1300 is much less active than the silver catalyst supported on this oxide. With an extension of the length of the isothermal segment to 6 h, the rate of soot combustion slightly changes. The final result is the same for both hold times.

The secondary electron microscope images of the series of alumina supports show how the support calcination temperature affects their topography (SI, Fig. S5A–G). When the support is calcined at 550 °C, the obtained oxide is highly porous. The sample calcined at 770 °C appears to be composed of larger agglomerates. A much more pronounced change is observed for the sample calcined at 900 °C. The samples heated at higher temperatures appear to have parts that are smooth and severely sintered. This is confirmed by the porosity studies of the sample (Fig. 2). The shape of the hysteresis loops, and hence pore types agree well with the differences in topography. The shape, very similar for the samples calcined at 550 °C and 700 °C, is altered due to calcination at 900 °C. The samples calcined at temperatures above 1000 °C are completely changed. The comparison of the hysteresis loops of the alumina supports calcined at 900, 1000 and 1100 °C and their respective catalysts shows that there is virtually no impact of the deposition of silver on the pore shape and size of the supports, only a slight decrease of the surface area (Fig. 2). There is a wide range of hysteresis loop shapes found for alumina calcined below 1000 °C in the literature despite similar calcination temperatures.[61–64]

The X-ray diffraction patterns of the alumina supports are compiled in Fig. 3A. Regardless of the calcination temperature, each diffraction pattern contains only one phase. Those calcined at 1000 °C or higher all have diffraction patterns typical for the stable, high-temperature polymorph. In contrast, those calcined at temperatures below 1000 °C showed that alumina was in one of its low-temperature polymorphic forms. The diffraction pattern obtained for the support calcined at 700 °C looks slightly different than that obtained at 900 °C, but is still a low-temperature polymorph. The diffraction patterns of the

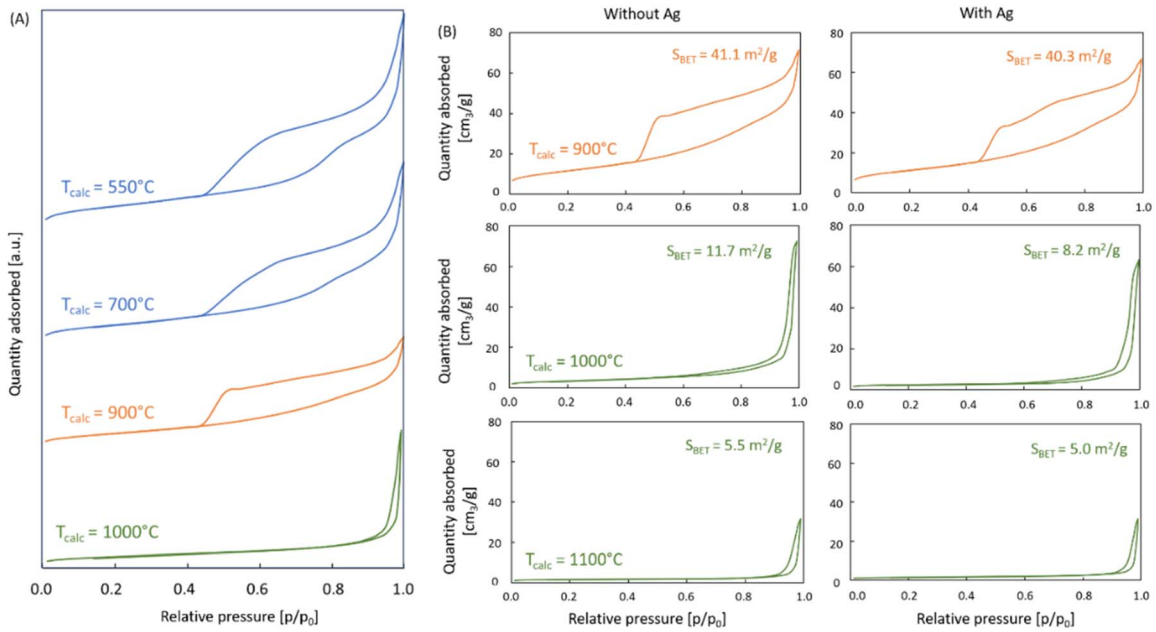

Fig. 2 The influence of (A) calcination temperature of alumina and (B) silver deposition on the porosity.

catalysts obtained with the high-temperature alumina polymorph contain silver only in the metallic form, as seen in Fig. 3B. This is not the case for low-temperature polymorphs. It can be seen that apart from metallic silver, the catalyst with the support calcined at 900 °C (Fig. 3C) contains both metallic silver and silver carbonate, as in the case of the catalyst obtained by our group previously whose support was calcined at 550 °C.[20] The peaks from silver carbonate and metallic silver are very narrow, which means that the crystallites are well formed. Silver carbonate thermally decomposes at temperatures substantially below T_{max} of soot combustion, as shown in our previous paper.[20] The most intensive peak of metallic silver is found at 38.1° (111), whereas the most intensive peak of silver carbonate is located at 33.6° (130). The increase of the ratio of these peaks is higher in Ag/Al-900 (Fig. 3C) than in Ag/Al-550 (SI, Fig. S8B). These results are in line with the results of the temperature programmed CO_2 desorption studies performed on this series of the catalysts, which show a decreasing trend in the quantity

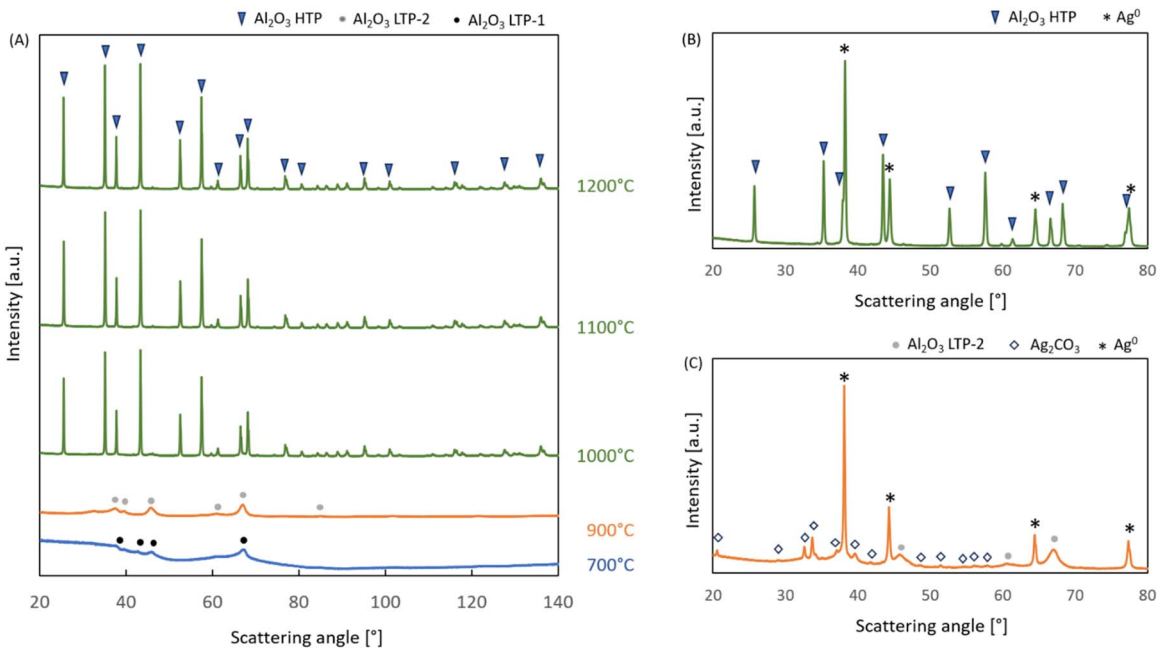

Fig. 3 Diffraction patterns of (A) the alumina supports calcined at different temperatures, (B) Ag/Al 1000 and (C) Ag/Al 900.

of the desorbed CO_2, especially that of the highest temperature peak (SI, Fig. S6). This trend is the same as that noted for the surface area, which can imply that although aluminum carbonate itself does not exist, the substantially higher surface area of the low temperature alumina samples can and do adsorb CO_2 from the air, which hence leads to silver carbonate formation upon deposition of silver from an aqueous silver nitrate solution. The presence of stable carbonate groups on the surface was confirmed by a very strong carbonate band in the FTIR spectra which was present despite the outgassing of the pressed pellet at 550 °C for 4 hours under vacuum, 5×10^{-4} hPa (SI, Fig. S8A).

The ChemiSEM image, the elemental maps and spectrum obtained for the catalyst supported on alumina calcined at 550 °C are shown in Fig. 4A. The ChemiSEM technology juxtaposes the SEM image with the elemental composition as determined with EDX. This image clearly shows that large yellow particles, *i.e.* metallic silver, are scattered on the purplish surface. There are no other particles on the surface, which is evidenced by a lack of dark spots. The same can be seen in the elemental maps: the blue map shows that the spots which have silver have relatively less oxygen than the alumina support (Fig. 4B). The aluminum maps also have dark spots where either a silver particle has covered it or where there is a pore. It should be emphasized that the spectrum shows no other elements (Fig. 4C). The map showing the silver distribution reveals the presence of silver in two forms (Fig. 4B): the large silver particles which are found on top of the surface and silver uniformly spread across the surface. In the light of the XRD data, it can be inferred that the uniformly spread form of silver is silver carbonate. However, carbon is an element which is always present in an EDX measurement, and on this surface, it is present in a very small amount (the peak is very low).

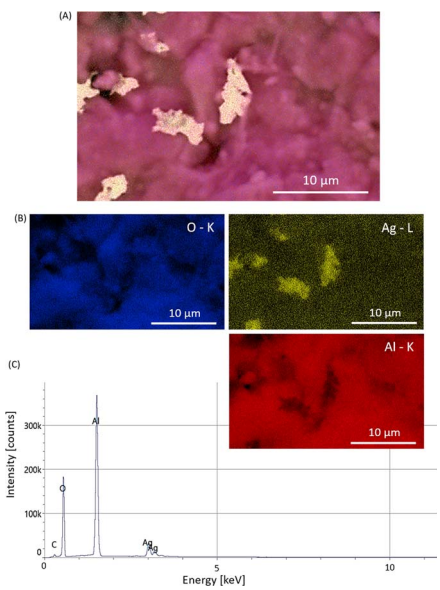

Fig. 4 EDX results: (A) ChemiSEM image of Ag/Al 550, (B) elemental maps of oxygen, aluminum and silver, and (C) EDX spectrum.

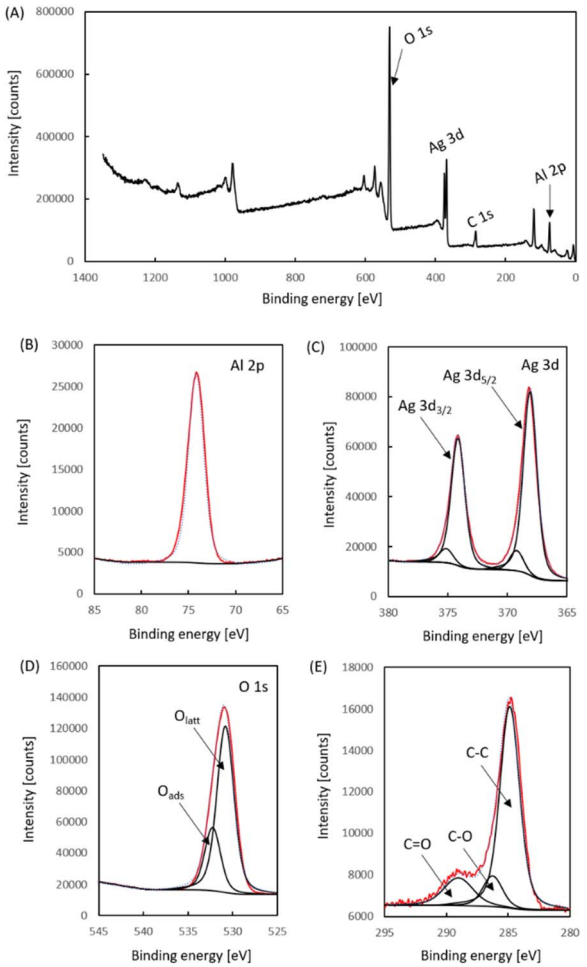

Fig. 5 XPS results for 15 wt% Ag/Al 550: (A) survey spectrum and detailed regions: (B) Al 2p, (C) O 1s, (D) C 1s and (E) Ag 3d; measurement points – red solid curve, envelope – blue dotted curve.

The purity of the surface of the catalyst was further probed with a surface sensitive technique, namely X-ray Photoelectron Spectroscopy (XPS). The results are depicted in Fig. 5. The survey spectrum (Fig. 5A) shows that the catalyst supported on alumina calcined at 550 °C does not contain any foreign elements. All of the peaks come from silver, aluminum and oxygen, as well as some adventitious carbon. The Al 2p region can be fitted with a single peak with a half width of 2.12 eV (Fig. 5B), despite the fact that in the low-temperature polymorphs of alumina the Al^{3+} ions are either in octahedral or tetrahedral coordination[65] and despite the fact that silver has been deposited onto it. The Ag $3d_{5/2}$ and $3d_{3/2}$ peaks (Fig. 5C) have a spin–orbit split of 6.0 eV and each can be fitted with two components. The rest of the detailed regions are very typical, namely O 1s can be fitted with the main lattice oxygen peak (O_{latt}) and an adsorbed oxygen peak (O_{ads}) on the high binding energy side of it (Fig. 5D), whereas the C 1s region can be fitted with three peaks (Fig. 5E), which correspond to: C–C (at 284.8 eV), C–O (at 285.0 eV) and C=O (at 288.2 eV).

The Hammett indicator tests were performed with samples after refreshing them by heating them to either 200 °C or 300 °C

and maintaining the temperature for 2 and 3 hours, respectively, to desorb any surface species which could interfere with the results of these tests. The results show that after regeneration at the higher temperature, all of the catalysts have the same range of active sites, but not after regeneration at the lower temperature. This is interesting as it shows that the acidic sites are more stable in the case of the alumina supports calcined at temperatures at or above 1000 °C.

The results of tests after each regeneration procedure (Table 1) show that the support calcination temperature influences the range of strength of acidic sites on the surface of aged alumina samples. The range of the strength of basic sites is the same for all of the samples regardless of the regeneration or support calcination temperature and falls in the range $7.2 \leq H^{-} < 15.0$. This means that none of the samples changed the color of the indicator whose pK_A value was 15.0. In contrast, the range of the strength of acidic sites is impacted by the regeneration temperature and the ease of regeneration changed with support calcination temperature. In the case of the higher regeneration temperature, all samples exhibit the same range of the strength of acidic sites, namely $-3.0 < H_0 \leq 4.8$. However, with the lower regeneration temperature, it can be seen that the three samples with the lower support calcination temperature do not possess available acidic sites. The alumina calcined at 1000 °C exhibits only the weakest acidic sites. In contrast, for the alumina samples calcined at a temperature of 1100 °C or higher, change can be observed for two Hammett indicators, resulting in a range of the strength of acidic sites denoted as follows: $-3.0 < H_0 \leq 4.8$. The fact that these results show a step-wise change in the acidity of the surface of the alumina supports calcined at 900 and 1000 °C may be a factor in the step-wise change of activity of Ag/Al-900 and Ag/Al-1000.

The Lewis and Brønsted acidity of the surface of Al-550 and the solid solutions was further investigated with transmission FTIR measurements using pyridine as the probe molecule (SI, Fig. S7). Prior to exposure to pyridine, the samples were heated to 550 °C in vacuum, which allowed the desorption of species from the surface. In the case of Al_2O_3 calcined at 550 °C it can be seen that even after desorption under vacuum, a pronounced band which corresponds to surface carbonates can be seen (SI, Fig. S7A). This abundance of carbonate species is in line with the CO_2-TPD results which show a large, high-temperature desorption peak for this sample. This is not the case for the CO_2-TPD curve of Al_2O_3 calcined above 1000 °C and no carbonate band can be seen in the FTIR spectrum of Al-1300 (SI, Fig. S7A).

The results of the pyridine-FTIR for selected supports, including those obtained with Al-550 and Al-1300, are compiled in Fig. S7B (SI). The pyridine is desorbed at temperatures between room temperature and 350 °C. The difference in the intensity of the band after desorption at room temperature and 150 °C is typically associated with the removal of physically bound pyridine. The results, *i.e.* bands associated with pyridine (approx. 1446 cm^{-1}), show a progressive decrease of the height/area of the pyridine band with a slight simultaneous shift to higher wavenumbers with increased desorption temperature for Al-550 (SI, Fig. S7C). Considering the height of the pyridine band left after desorption at 300 °C, it can be stated that the concentration of strong Lewis sites (typically calculated based on the band at 350 °C) is low regardless of the calcination temperature. The binding of pyridine is stronger on the surface of Al-550 than on Al-1300 which can be seen by a more pronounced decrease of the band intensity with increased desorption temperature. In the case of Al-1300 all of the pyridine is desorbed at 150 °C and the curve goes back to the baseline (SI, Fig. S7D). Moreover, these two samples differ in the concentration of pyridine on the surface due to a much higher surface area of Al-550, although caution should be taken when directly comparing the intensity of bands between different samples measured in transmission mode as pellets may differ in thickness. The pyridine studies show no visible bands associated with Brønsted acidity.

Table 1 Hammett indicator test results of undoped alumina

	pK_{BH^+}/pK_A					
Sample	−3.0	0.8	4.8	7.2	9.3	15.0
$T_{reg.}$ [°C]	200/300	200/300	200/300	200/300	200/300	200/300
Al-550	−/−	−/+	−/+	+/+	+/+	−/−
Al-700	−/−	−/+	−/+	+/+	+/+	−/−
Al-900	−/−	−/+	+/+	+/+	+/+	−/−
Al-1000	−/−	+/+	+/+	+/+	+/+	−/−
Al-1100	−/−	+/+	+/+	+/+	+/+	−/−
Al-1200	−/−	+/+	+/+	+/+	+/+	−/−
Al-1300	−/−	+/+	+/+	+/+	+/+	−/−

3 Alumina-based solid oxide solutions

3.1 Solid solutions calcined at 550 °C

Solid solutions containing cobalt, cerium and chromium guest ions in the host oxide, alumina, were obtained with a dopant: Al^{3+} ratio of 1 : 9. As in the case of the undoped alumina supports, the labels used in this section contain the symbol "Al", followed by the symbol of the dopant, a dash and the support calcination temperature in degrees Celsius, *e.g.* AlCr-550 is used to denote the chromium-doped alumina support calcined at 550 °C. It is noteworthy that the XRD patterns indicate that all three solid solution supports calcined at 550 °C are composed of the same low-temperature polymorph as the undoped alumina calcined at 900 °C (SI, Fig. S8A, red rectangles).

The temperature of the maximum soot combustion with the Co-doped alumina support is the same as that of soot alone (602 °C, Fig. 6A) indicating that this solid solution does not catalyze the reaction. The cobalt-alumina spinel, known as cobalt blue, in which Co^{2+} ions are coordinated in tetrahedral sites and Al^{3+} is found in the octahedral sites, is commonly obtained with a much higher cobalt to aluminum ratio and is typically acquired at much higher temperatures,[33] but in the current work, the solid solution was a vibrant blue despite the

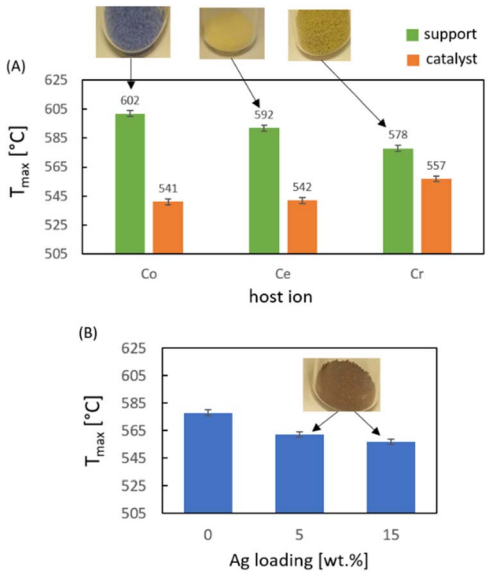

Fig. 6 Temperature of the maximum soot combustion rate determined for: (A) supports calcined at 550 °C and the respective catalysts, and (B) catalysts with different silver loadings supported on AlCr-550.

low calcination temperature (Fig. 6A). XPS analysis showed that the cobalt in the support is present in the form of Co^{2+} (SI, Fig. S9A) with intensive satellite peaks approx. 6 eV from the main Co 2p peaks. The blue color is typically attributed to $CoAl_2O_4$, whereas in our studies the Co : Al ratio was 1 : 9, not 1 : 2. An addition of Co_2AlO_4 is said to make the pigment greener, whereas the presence of Co_3O_4 is said to make it darker.[33] In our case, there was no other phase in the cobalt-doped alumina calcined at 550 °C (SI, Fig. S8A) and no other element seen in the XPS survey spectrum (SI, Fig. S9B).

The cerium-doped support has a slightly lower T_{max} value (592 °C) temperature than that noted for uncatalyzed soot combustion. The XRD pattern of AlCe-550 reveals the presence of peaks from CeO_2 as well (SI, Fig. S8A). However, it is known that even small concentrations of CeO_2 give relatively very intensive peaks in the diffraction patterns. Despite the presence of CeO_2, the T_{max} observed for AlCe-550 is substantially higher than that noted for the chromium-doped support, AlCr-550 (578 °C). The XPS spectra reveal no other elements in AlCe-550 (SI, Fig. S8B). The value observed for AlCr-550 is the only one which is noticeably below the temperature observed for uncatalyzed combustion of the model soot used in these studies (602 °C). Since the XRD studies do not show the presence of any chromium-containing phase (SI, Fig. S8A), this means that all of the chromium is incorporated into the alumina host. Moreover, there are no foreign elements, as shown in the survey spectrum of the support (SI, Fig. S9C). Hence, it is the incorporation of chromium into the alumina lattice which is responsible for the considerable improvement in the activity.

The deposition of 15 wt% silver onto these catalysts results in a substantial decrease of the temperature of the maximum soot combustion rate (Fig. 6A) regardless of the host ion. Interestingly, the least active catalyst (Ag/AlCr-550) is the one supported on the most active support. In the case of this catalytic system, the decrease in T_{max} upon silver deposition is only 21°, whereas for the catalysts supported on AlCe-550 and AlCo-550, the decrease of T_{max} equals 50 and 58°, respectively and the resulting T_{max} is the same for those two catalysts (within experimental error). It must be emphasized that the addition of a guest ion alone has significantly improved the activity of the low-temperature alumina. Nevertheless, the silver particles supported on the low-temperature solid oxide solutions show the same behavior as Ag/Al-550 during a catalytic measurement, namely a change in both the shape and size of particles (SI, Fig. S2E and F).

The thermogravimetric tests without soot have shown that the curves of Ag/AlCe-550 and Ag/AlCo-550 (SI, Fig. S1C and D, respectively) look the same as that obtained for Ag/Al-550. In contrast, the results of the TG-MS study with Ag/AlCr-550 (SI, Fig. S1E and F) has revealed that there is a decrease of the mass of the sample, which is also true for the support itself. The MS data indicate that there are no changes of the curves for any of the four monitored m/z ratios, namely: 28 (N_2 or CO), 32 (O_2), 18 (H_2O) or 44 (CO_2) due to this transition. It is important that these are not impacted, which means that neither oxygen is consumed nor CO_2 forms during this transition. The most likely explanation for the mass loss is the elimination of CrO_3, the oxide of chromium(VI) is volatile and is the component in Ag/AlCr-550 which is responsible for the formation of Ag_2CrO_4 (SI, Fig. S8B). A test with the spent catalyst in a second cycle showed a slight change of the DTG curve (SI, Fig. S3B).

In order to determine if the relatively small improvement of activity of the chromium-doped solid solution upon silver deposition is a result of an excessively high silver loading, another catalyst with 5% silver was obtained. However, the result was a lower activity, *i.e.* higher T_{max} than that noted for the catalyst with 15 wt% Ag (Fig. 6B). In the case of the chromium-doped support, both of these two turned bright red upon silver deposition due to the formation of silver chromate, as shown in the XRD pattern (SI, Fig. S8B). The crystallites of this phase are large, probably >100 nm, but contain substantial defects. This is unlike the other catalysts which contain metallic silver and silver carbonate (SI, Fig. S9B).

The XPS spectra of the catalyst supported on undoped alumina calcined at 550 °C have shown that there are no impurities on the surface and that the Al 2p peak can be fitted with a single component, *i.e.* there are no shoulders associated with a different chemical environment of aluminum ions (Fig. 7A), even after the deposition of silver (Fig. 5B). This, however, was not the case for the solid solutions. All three supports, namely AlCr-500 (Fig. 7B), AlCe-550 (Fig. 7C) and AlCo-550 (Fig. 7D) have an additional component equal to 12, 13 and 10%, respectively, on the high binding-energy side. The smaller peak is separated by 1.3–1.4 eV from the main peak. The fact that these two components are similar for all three supports further confirms that the incorporation of chromium, cerium or cobalt ions into the alumina lattice impacts the chemical environment of the aluminum ions. In the case of the chromium-doped support the deposition of silver does not influence the Al 2p region (Fig. 7E). In contrast, when silver is

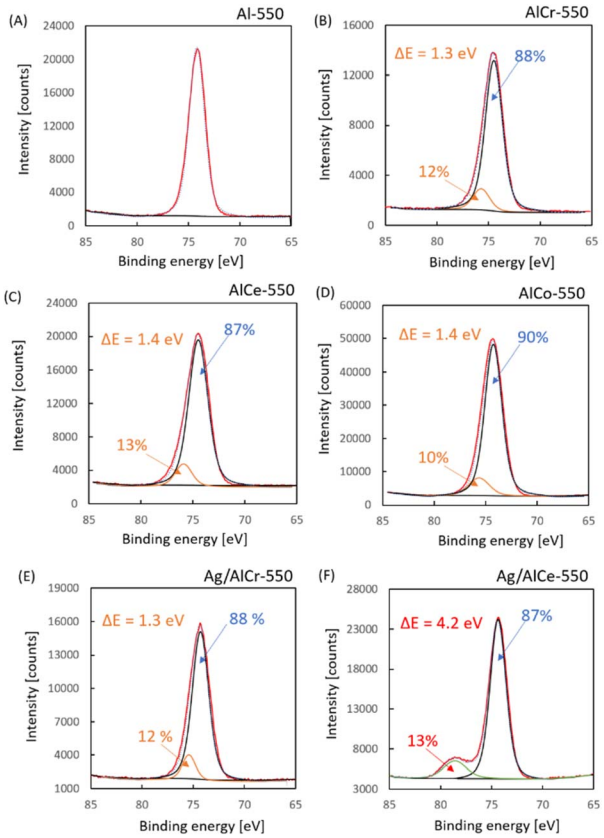

Fig. 7 The detailed Al 2p regions of: (A) Al-550, (B) AlCr-550, (C) AlCe-550, (D) AlCo-550, (E) Ag/AlCr-550 and (F) Ag/AlCe-550; measurement points – red solid curve, envelope – blue dotted curve.

deposited onto AlCe-550, the shoulder further shifts to become a peak with 13% of the area and which is separated by 4.2 eV from the main aluminum peak. Since the ratio of the two peaks is the same as in the support itself, it can be postulated that the chemical environment of those Al^{3+} species which are slightly different in the support are further modified by the interaction with silver. The difference between these two samples may indicate that in the chromium-doped alumina, the formation of silver chromate does not influence the chemical environment of the aluminum ions, whereas the silver on the cerium-doped alumina interacts differently with the two types of Al^{3+} ions causing an even more pronounced difference in the binding energy. A study to investigate the matter is underway. Nevertheless, the XPS studies clearly show that the surface aluminum ions are changed in the presence of foreign ions incorporated into the support.

The CO_2-TPD studies of the solid solutions show some similarities between the undoped alumina and the doped samples. Fig. 8A contains the desorption curves of AlCr-550 (blue curve) and Ag/AlCr-550 (black curve) which have the same low-temperature peak as the catalyst supported on Al-550 (purple curve) whose maximum is at 90 °C. The deposition of silver does not impact the position nor the area of the peak. The same peak is observed in the cerium-doped sample (Fig. 8B). This peak is much bigger than in the case of the chromium-

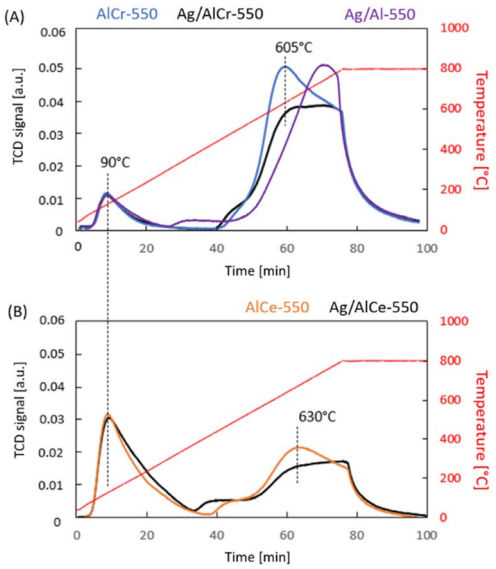

Fig. 8 CO_2-TPD study results of: (A) AlCr-550, Ag/AlCr-550 and Ag/Al-550 and (B) AlCe-550 and Ag/AlCe-550.

doped support, though again, its position and shape is not affected by silver deposition. The high-temperature peak, however, is clearly shifted to lower temperatures than in the undoped alumina: to 605 °C for AlCr-550 and 630 °C for AlCe-550, respectively. This peak is much higher for AlCr-550 than for AlCe-550. In fact, the shape of the desorption curve of CO_2 from AlCe-550 resembles that of Al-900 rather than that of Al-550. In both cases the deposition of silver leads to a decrease of the concentration of strongly bound CO_2. This is interesting considering the fact that silver is in different forms on these supports: silver chromate on AlCr-550 and a mixture of metallic silver and silver carbonate on AlCe-550 (SI, Fig. S8B). This shows that the insertion of a dopant into the alumina lattice alters the basicity of the obtained solids. It is noteworthy that a substantially smaller high-temperature desorption peak in AlCe-550 than in undoped alumina corresponds well with a smaller relative abundance of silver carbonate in the resulting catalyst calculated based on their diffraction patterns. The choice of the dopant leads to more pronounced changes than the deposition of silver. The results show that the basicity of the system as measured by CO_2-TPD does not seem to be a major contributing factor for the overall activity of the systems.

In Tof-SIMS studies the surface of the alumina catalysts is actively probed by bombarding it with primary ions in order to see what secondary ions are ejected. The "matrix effect", often referred to as a flaw of the method, is treated as an advantage in this study. The "matrix effect" results in different ratios of secondary ions when the chemical environment of ions is different. The differentiation of the environment of ions by changes in the calcination temperature of alumina is exactly what we wanted to probe. The results are compiled in Fig. 9A. Considering the support composition, the ions which can be emitted from the surface and observed in the negative ion spectrum, apart from O^- ($m/z = 16$) and Al^- ions ($m/z = 27$), are

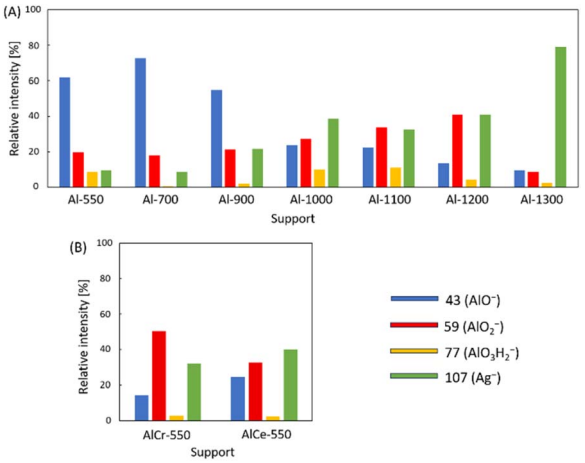

Fig. 9 ToF-SIMS study results of: (A) alumina-supported silver catalysts and (B) Ag/AlCr-550 and Ag/AlCe-550.

(1) AlO^-, $m/z = 43$, (2) AlO_2^-, $m/z = 59$, and (3) $AlO_3H_2^-$, $m/z = 77$, as well as (4) Ag^-, $m/z = 107$. These were used to create a peak table so that relative abundances rather than absolute values could be used for evaluation. As in the case of the Hammett indicator tests, the ToF-SIMS measurements also discriminate between the surface of the catalysts supported on alumina calcined at 900 °C or below and those calcined at 1000 °C or above. For catalysts supported on alumina calcined at 900 °C or below, the most abundant from the four selected peaks is AlO^-, but it is not the dominant fragment in the spectra of Ag/Al-1000, Ag/Al-1100, Ag/Al-1200 or Ag/Al1300. The fact that the fragments with the Al : O ratio of 1 : 1 and 1 : 2 are equally likely to be emitted in the latter group speaks about the interaction of aluminum ions with the anion sublattice. It is also noteworthy that a second trend can be seen is the increase of the ease of extraction of Ag^- ions with increasing calcination temperature. The ToF-SIMS results of catalysts supported on chromium-doped (AlCr-550) and cerium-doped (AlCe-550) supports show that for these systems, the relative ratios of AlO^- ($m/z = 43$) and AlO_2^- closely resemble those observed for catalysts supported on alumina calcined at temperatures at or above 1000 °C.

In contrast to the CO_2-TPD results, which show that the chromium-doped sample has strongly bound surface carbonate, the FTIR spectrum obtained after desorption under vacuum at 550 °C of AlCr-550 shows no carbonate bands (SI, Fig. S7A). This implies that unlike the undoped Al_2O_3 calcined at 550 °C, the surface carbonates on AlCr-550 are much less stable under reduced pressure. The lack of carbonate bands was noted also for the Co-doped and Ce-doped solid solutions after desorption at 550 °C under vacuum. The FTIR studies have shown that all three oxide solutions calcined at 550 °C give similar spectra both prior after and after pyridine adsorption (SI, Fig. S7A and B, respectively). A closer look at the desorption curves, as shown in the example of AlCe-550 (SI, Fig. S7E) reveals that the desorption of pyridine from the surface of the solid solutions occurs in the same manner as in Al-550.

Table 2 Hammett indicator test results of the doped-alumina supports

Sample		AlCr-550	AlCo-550	AlCe-550
Blank		Brown	Dark blue	Light yellow
H_0 (pK_{BH^+})	−3.0	Brown	Dark blue	Light yellow
	0.8	+	+	+
	4.8	+	+	+
H^- (pK_A)	7.2	Brown	Dark blue	+
	9.3	Brown	+	+
	15.0	Brown	—	—

However, the shape changes due to a relatively higher concentration of strong Lewis sites.

The Hammett indicator tests performed with the solid solutions regenerated at both temperatures gave the same results revealing that in comparison to the undoped alumina supports, these supports have more stable/easier to regenerate acidic sites. The results are compiled in Table 2. Since the different indicators turn different colors and AlCr-550 turned brown in several cases, which is not an option for any of the indicators, a blank test was performed with anhydrous toluene. When the change was visible for a certain support with a given indicator, the table contains a plus. However, some color changes were not discernible due to the color of the supports. Hence, when the color change was difficult to assess, the color itself was put into Table 2.

The chromium-doped solid solution calcined at 550 °C (AlCr-550) reacts with the toluene itself, yet a clear change in the presence of the indicators with pK_{BH^+} of 0.8 and 4.8 to the proper colors were observed (Table 2). In fact, transitions with these two indicators were visible for all of the studied samples. One interesting fact is that the intensive color of AlCo-550 hinders the assessment of the indicator with pK_A value of 7.2, but since the next one changed color, it is inferred that sites with the lower strength are also present. What is paramount in these results is the fact that the acidic sites are stable when chromium, cobalt or cerium ions are inserted into the alumina structure and the lower regeneration temperature was sufficient, same as for undoped alumina supports calcined at high temperatures.

3.2 Solid solutions calcined above 550 °C

In order to obtain a catalyst supported on chromium-doped alpha alumina, the green AlCr-550 (Fig. 10A) was heated to 1000 °C. Although this temperature was sufficient to obtain the high temperature polymorph in the case of undoped alumina, it was not high enough for the chromium-doped sample, as evidenced by the comparison of the standard for alpha Al_2O_3 and the diffraction pattern of AlCr-1000 (SI, Fig. S10A and B, respectively). This sample exhibits a much higher crystallinity than AlCr-550, but it is not the high temperature polymorph. For clarity, the diffraction peaks of the standard were extended with dashed lines all the way to the bottom of the figure to elucidate which peaks comes from alpha alumina. No color change from green occurred, only of the shade (Fig. 10A). The

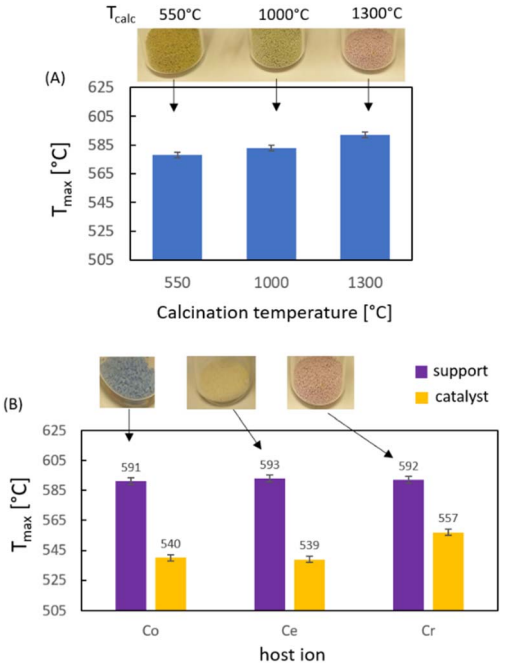

Fig. 10 Temperature of the maximum soot combustion rate determined for: (A) chromium-doped supports calcined at different temperatures and (B) supports calcined at 1300 °C and the respective catalysts.

calcination temperature for this support was increased in intervals of 100° and after calcination at 1300 °C the diffraction pattern of the alpha alumina (SI, Fig. S10C) was observed along with a color change to pink (Fig. 10A). This is why the other two supports were also calcined at 1300 °C, which showed to be sufficiently high to yield alpha alumina in both (SI, Fig. S10C). The higher support calcination temperature appears to allow the non-incorporated CeO_2 to form well-defined crystals which yield very intensive peaks in the XRD analysis.

The activity of the chromium-doped supports themselves decreased upon increase in T_{calc}, which is different than what was observed for the undoped alumina catalysts (Fig. 10A). One possible explanation is the change in the oxidation state and/or coordination of the chromium ions in the alumina host matrix. It is known that in α-alumina chromium is present in the form of Cr^{3+} in octahedral coordination, *i.e.* in rubies.[34] In the case of the support with the low calcination temperature, additional studies are underway to determine the types of chromium ions present and their location in the host structure. Nevertheless, the measurements without soot have revealed that unlike AlCr-550, neither AlCr1300 nor Ag/AlCr-1300 exhibit mass loss (SI, Fig. S1G and H). The isothermal activity tests with the three-hour-long isothermal segments indicate that in the presence of Ag/AlCr-1300 (Fig. S4D) the majority of the soot combusts within the first isothermal segment and there is no additional mass loss as in the case of Ag/AlCr-550, as in the tests without soot. Moreover, the rate of soot combustion is slower than that seen with Ag/AlCr-550.

It is noteworthy that all of the supports calcined at 1300 °C have the same T_{max} and all exhibit the alpha-alumina structure (Fig. 10B, purple bars). Apart from the change in the polymorphic form of the alumina, the high-temperature support calcination did not lead to the formation of any new phases in the case of chromium-doped alumina, nor the cerium-doped alumina. Only for the cobalt-doped support, the formation of another phase, namely Co_3O_4, was detected (SI, Fig. S10C). It is interesting that despite the presence of Co_3O_4, the support was a lighter shade of blue, not darker, as implied by other studies.[33]

The catalysts obtained with supports calcined at the higher temperature exhibit very similar activity (Fig. 10B, yellow bars) to those noted for the catalysts with the corresponding supports calcined at 550 °C. In short, our studies have revealed that high temperature treatment of these supports was not beneficial for the activity of the obtained silver catalysts in soot oxidation. Therefore, further studies are planned with different dopants at a low calcination temperature to tailor the properties of the low-temperature polymorphs of alumina rather than influencing the activity of such systems by a high-temperature treatment and subsequent change to alpha alumina.

The elemental maps of AlCo-1300 (Fig. 11A) show that in the case of the cobalt-doped support, the calcination to 1300 °C leads to the formation of cobalt-enriched particles on the surface. Since the XRD results show the presence of Co_3O_4 and the map of oxygen does not show depletion in oxygen, it can be inferred that the particles seen in the cobalt elemental map and the CBS image (Fig. 11C) are those of Co_3O_4. In contrast, the elemental maps of AlCe-1300 (Fig. 11B) reveal an even distribution of cerium across the surface. The fact that a part of the cerium ions is present as the solid oxide solution but a part is

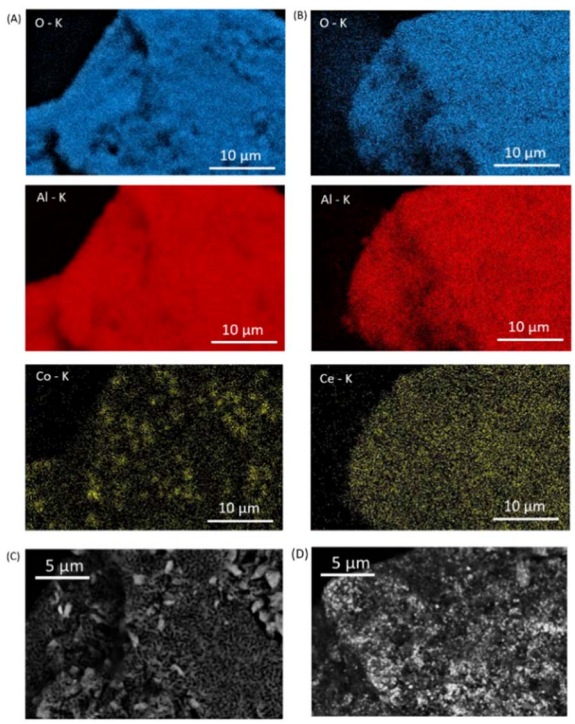

Fig. 11 SEM-EDX results: elemental maps (A and B) and backscatter electron images (C and D) of AlCo-1300 and AlCe-1300, respectively.

present as CeO_2, even after support calcination at 550 °C, would suggest that the ceria particles should be very large after further calcination at 1300 °C. However, only small, discrete particles of a heavier compound can be seen in the CBS images. Indeed, these particles are much smaller than those of Co_3O_4 found on the surface of AlCo-1300.

The results of Hammett indicator tests for the doped samples calcined at temperatures higher than 550 °C (SI, Table S1) indicate a small influence of the increased calcination temperature on the acid–base properties of these solid solutions. The results did show that in contrast to AlCr-550, the sample AlCr-1000, which is also green, did not turn brown in anhydrous toluene, which may suggest that it does not contain as many oxidation states of chromium as the sample calcined at 550 °C. Moreover, it was seen to turn pink in the presence of phenolphthalein. This transition was also observed for AlCe-1300.

The FTIR spectra of the supports calcined at 1300 °C are similar to those of Al-1300 (SI, Fig. S7A). Considering the high calcination temperature, and hence the decrease of surface area it is logical that the degassed samples would exhibit relatively fewer functional groups as well as less pyridine would be adsorbed (SI, Fig. 8B). However, the pyridine tests have revealed that the high-temperature solid oxide solutions have stronger bound sites than undoped alumina (SI, Fig. S7F). This is evidenced by the fact that the undoped alumina loses all of the pyridine during the desorption at 150 °C, whereas AlCe-1300 still has a visible band at 1444 cm^{-1} after pyridine desorption at 150 °C and also 200 °C.

4 Experimental

4.1 Materials and methods

4.1.1 Supports. The undoped alumina samples were prepared by thermal decomposition of aluminum nitrate (analytical grade, POCh Gliwice). They were calcined for 4 hours at different temperatures: 550 °C, 700 °C, 900 °C, 1000 °C, 1100 °C, 1200 °C and 1300 °C. These are labelled as: Al-550, Al-700, Al-900, *etc.* The calcination temperature in every symbol, including those of the catalysts, refers to the calcination temperature of the support.

The solid solutions were synthesized using the following reagents: aluminum nitrate nonahydrate (analytical grade, POCh Gliwice), ammonium ceric(IV) nitrate (analytical grade, Pol-Aura), cobalt(II) nitrate hexahydrate (analytical grade, POCh Gliwice) and chromium(III) nitrate hexahydrate (analytical grade, POCh Gliwice). A dopant to aluminum molar ratio of 1 : 9 was applied. The salts were dissolved in deionized water, mixed and precipitated with excess ammonia water (25%, POCh Gliwice) under stirring. The obtained gel was washed to a pH of 7, dried at 200 °C for two hours and calcined at 550 °C for four hours. Next, the grains with the average size between 0.230 and 0.500 mm were obtained. The same procedure was used to obtain undoped alumina.

4.1.2 Catalysts. The supports were impregnated with an aqueous solution of silver nitrate (analytical grade, POCh, Gliwice) containing 0.27 g of silver nitrate per gram of catalyst to obtain a final loading of approximately 15 wt%, dried for 2 h at 150 °C and calcined at 550 °C for an hour. The final calcination of the catalyst after silver nitrate deposition was 550 °C regardless of the support calcination temperature. Therefore, the symbol Ag/AlCr-1300 is used for the silver catalyst obtained using the chromium-doped alumina support which was calcined at 1300 °C onto which silver nitrate was deposited and calcined at 550 °C.

4.2 Activity studies

The activity experiments were performed using an STA 449C (NETZSCH) thermobalance with a mass spectrometer (QMS 403C, NETZSCH) in the DTA-TGA mode. Prior to a measurement the samples were ground for one minute in an agate mortar with soot (a 5 : 1 ratio) and approx. 30 mg were weighed out into a crucible, which was kept at 30 °C for 30 minutes in a flow (90 mL min^{-1}) of synthetic air (5 N, Multax). They were conducted in synthetic air with a steady temperature ramp of 10 degrees per minute up to 850 °C.

Additional measurements in accordance with the same temperature program were conducted without soot in either the TG or TG-MS mode to determine if the calcined catalysts remain unchanged in the studied range of temperatures.

Cycling activity tests were also performed in order to test the stability of the catalytic activity, in which a catalyst used for an activity test was reused by grinding it with another portion of soot.

Isothermal experiments were completed with one of two temperature programs. Both were carried out with approx. 30 mg of a sample of a 5 : 1 catalyst/support to soot ratio obtained by grinding the sample with soot for one minute in an agate mortar. Isothermal Program 1 (Iso1) consisted of the following steps: (1) heating to 420 °C at a ramp of 10 degrees per minute, (2) isothermal hold for 3 hours, (3) heating for two minutes at a rate of 10 degrees per minute, (4) isothermal hold for 3 hours, (5) repeating steps 3 and 4 until the isothermal hold at 480 °C was completed. Isothermal Program 2 (Iso 2) was comprised of the following steps: (1) heating to 420 °C at a ramp of 10 degrees per minute, (2) isothermal hold for 6 hours, (3) heating for two minutes at a rate of 10 degrees a minute, (4) isothermal hold for 6 hours.

4.3 Characterization studies

4.3.1 Temperature programmed desorption of carbon dioxide (CO_2-TPD) and H_2 (H_2-TPD) studies. The CO_2-TPD and H_2-TPD determinations were performed with an Autochem 2920 instrument from Micromeritics equipped with a Thermal Conductivity Detector using approx. 0.15 g and 0.30 g of a sample, respectively. The CO_2-TPD measurements were done in accordance with the following procedure: the sample was flushed with helium at 500 °C flowing at 40 mL min^{-1} for 1 h, then the sample was cooled to 40 °C and was dosed with a 9 : 1 He–CO_2 mixture (40 mL min^{-1}) for 2 h, next, it was flushed with flowing helium for 1 h (40 mL min^{-1}) and the measurement was carried out with a heating ramp of 10 °C min^{-1} to 800 °C, followed by a 25 minutes isotherm. Prior to the H_2-TPD

measurements the oxidized forms of silver in the samples were thermally decomposed to metallic silver by increasing the temperature to 550 °C at a rate of 30 degrees per minute in flowing argon (40 mL min^{-1}), hold time of 120 minutes, followed by cooling to 150 °C at a rate of 10 degrees per minute. Next, the sample was dosed with hydrogen while being cooled to 0 °C and for 15 minutes after that temperature was reached. Next, the sample was flushed with flowing argon until the baseline was stable. The sample was then heated to 800 °C at a rate of 10 degrees per minute in flowing argon. External calibration curves were obtained prior to measurements and used for quantification.

4.3.2 X-Ray diffraction studies. The XRD studies were performed on a Siemens D 5000 diffractometer (Bruker AXS GmbH) using a copper X-ray tube which operated at 40 kV, 40 mA. The diffraction patterns were recorded within the 2θ range of 20–140° using a 0.02 angular resolution. Rietveld analysis was used for the refinement of structures of the crystalline phases.

4.3.3 Scanning electron microscopy (SEM) – energy dispersive X-ray spectroscopy (EDX) studies. Two microscopes from ThermoScientific were used for this study: Prisma E and Helios 5 PFIB. In both cases the topography was probed with an Everhart-Thornley Detector and the homogeneity of the samples was determined using a Circular Backscatter Detector. Moreover, Prisma E has a feature called ChemiSEM™ Technology, which compiled the SEM image of a given surface with the chemical information from the EDX measurement. The measurements were performed with the acceleration voltage of 15 kV. Magnifications between 500 and 10 000 times were used.

4.3.4 Time-of-flight secondary ion mass spectrometry (ToF SIMS) studies. Helios 5 PFIB was applied for Time-of-Flight Secondary Ion Mass Spectrometry using a Xenon ion gun as the source of primary ions. The parameters were: 4 nA current, 30 kV voltage, 512 × 442; 50 μm horizontal field width (HFW) and 10 μs dwell time. The analysis of negative and positive ion spectra was performed with ToF-SIMS Explorer v. 1.12.2.0 from Tofwerk.

4.3.5 Hammett indicator tests. The following indicators were used for probing the acidic sites (the pK_{BH^+} value of each is given in parentheses): chalcone (−5.6), dibenzylideneacetone (−3.0), crystal violet (0.8) and methyl red (4.8). The following indicators were used for probing the basic sites (the pK_A value of each is given in parentheses): bromothymol blue (7.2), phenolphthalein (9.3) and 2,4-dinitroaniline (15.0), 4-nitroaniline (18.4), diphenylamine (22.3), 4-chloroaniline (26.5) and triphenylmethane (33.0). Prior to performing the experiments, the samples were refreshed to desorb any adsorbed species with a thermal treatment. Two thermal treatments were applied in sequence: Treatment 1, in which the samples were heated and kept at 200 °C for 2 hours and Treatment 2, in which the samples were heated to 300 °C and kept at that temperature for 3 hours. Directly after the thermal treatment approximately 30 mg of the samples were placed in vials and four drops of the 0.1 wt% toluene solutions of the indicators were added. The color of the grains of the catalyst was determined after 24 hours to allow the indicator color to develop.

4.3.6 Fourier transform infrared spectroscopy studies. Two spectrometers from ThermoScientific were used for this study: the ATR-FTIR measurements were performed with Nicolet iS5 using the iD7 ATR ad-on, whereas the transition mode experiments were conducted using a Nicolet 6700 instrument. The preliminary ATR-FTIR studies were carried out in the wavenumber range 500–4000 cm^{-1} (16 scans). The pyridine adsorption studies were performed in transmission mode on the Nicolet 6700 apparatus equipped with a furnace, liquid nitrogen traps, $CaCl_2$ windows and a quartz holder in which the wafer was held during heating and measurements. A mechanical lift shaft was used to move the holder with the sample between the heating zone and the path of the beam. Prior to measurements a pellet was made using approx. 20 mg of the alumina powder pressed using a pressure of 40 MPa. The sample was placed in a quartz holder and heated to 550 °C for degassing for 4 hours at a pressure of 4×10^{-4} hPa. Next, the sample was cooled to room temperature, a spectrum was collected and the sample was exposed to pyridine for 5 minutes. The pyridine was desorbed at the following temperatures: room temperature, 150, 200, 250 and 300 °C with 10 minutes holding time at each temperature. A spectrum was collected after cooling with 24 scans, recorded in the range of wavenumbers 1300–4000 cm^{-1}.

4.3.7 Nitrogen physisorption studies. Nitrogen physisorption studies were conducted on a Micromeritics ASAP 2020 instrument at liquid nitrogen temperature (77 K). Samples were pre-treated under vacuum (500 μm Hg) for 60 minutes, then the temperature was increased to 150 °C and maintained for 240 minutes prior to the cool-down and subsequent measurement. The surface area was calculated using the Brunauer–Emmett–Teller (BET) equation. The adsorption–desorption isotherms data was collected in the p/p_0 range of 0.01–0.99.

4.3.8 X-ray photoelectron spectroscopy (XPS) studies. XPS measurements were performed on an X-ray photoelectron spectrometer, model K-Alpha, from ThermoScientific equipped with a monochromated Al X-ray source operating in the Fixed Analyzer Transmission mode. A flood gun was used for charge compensation. Prior to the measurements the samples were placed on the holder using double-sided graphite tape and subjected to evacuation in an ultra-high vacuum. A 250 μm spot size was used. The survey spectra were obtained with a pass energy of 100 eV, 15 scans. The following detailed regions were acquired with a 0.1 eV step: C 1s, O 1s, Al 2p, Ag 3d, Co 2p, Cr 2p and Ce 3d. The peaks were fitted using Avantage 5.982 software from ThermoScientific. The spectra were shifted to align the binding energy of the main C 1s peaks to 284.8 eV and the aluminum oxide Al 2p peaks were fitted by a single component rather than with two spin–orbit components as with metallic Al (as suggested by ThermoScientific analysis software).

5 Conclusions

A series of alumina supports were obtained at different calcination temperatures. Silver was deposited onto them and DTA-TGA measurements were conducted to assess the activity of the obtained catalysts in tight-contact soot combustion. T_{max} of the

DTA curve, which was used to compare the activity of the systems, showed that the catalysts supported on α-alumina exhibited higher activity than the catalyst supported on the low-temperature alumina polymorphs. The enhancement in activity was a step-wise change. Though several parameters changed gradually with alumina calcination temperature and therefore cannot be held accountable for the difference, the results of ToF-SIMS studies and Hammett indicator tests both revealed a yes/no-type of change between the catalysts supported on the low-temperature polymorphs and on the high-temperature one. Interestingly, the three solid solutions with the Al^{3+}:dopant ratio of 9 : 1 which were calcined at 550 °C prior to silver deposition, yielded more active catalysts than the one supported on alumina calcined at this temperature. In fact, the catalysts on doped-alumina supports calcined at 550 °C exhibited similar activity to the catalysts supported on α-alumina, though they contained a low-temperature polymorph of Al_2O_3. However, the ToF-SIMS and Hammett indicator tests pointed to the similarities of the catalysts with doped-alumina supports to Ag/α-alumina rather than catalysts on low-temperature alumina polymorphs. An increase in the calcination temperature of the doped-support to 1300 °C did not result in an improvement of activity despite the transition of the supports to α-alumina.

Author contributions

Conceptualization, E. M. I.; methodology, E. M. I.; validation, E. M. I.; formal analysis, E. M. I.; investigation, E. M. I., A. G., P. W., P. F., M. D. and W. P.; resources, E. M. I.; data curation, E. M. I.; writing—original draft preparation, E. M. I.; writing—review and editing, E. M. I.; visualization, E. M. I.; supervision, E. M. I.; project administration, E. M. I.; funding acquisition, E. M. I. All authors have read and agreed to the published version of the manuscript.

Conflicts of interest

There are no conflicts to declare.

Data availability

The data supporting this article have been included as part of the supplementary information (SI). Supplementary information: Fig. S1: Thermal analysis results for (A) Ag/Al-550, (B) Ag/Al-1300, (C) Ag/AlCe-550, (D) Ag/AlCo-550, (E) Ag/AlCr-550, (F) MS data for Ag/AlCr-550, (G) Ag/AlCr-1300 and (H) AlCr-1300; Fig. S2: Backscattered electron images of catalysts before and after soot combustion: (A) fresh Ag/Al-550, (B) spent Ag/Al-550, (C) fresh Ag/Al-1300, (D) Ag/Al-1300 after 6 catalytic cycles, (E) fresh Ag/AlCe-550 and (F) spent Ag/AlCe550; Fig. S3: Cycling soot combustion test results of (A) Ag/Al-1300 and (B) Ag/AgCr-550; Fig. S4: ICP measurement results: Ag, Cr and Y lines obtained for the following fresh and spent catalysts (A) Ag/Al-1300, (B) Ag/AlCr-550 and (C) Ag/AlCr-1300; Fig. S5: Isothermal soot combustion results of (A) Ag/Al-1300 (black curve) and Al-1300 (orange curve), (B) Ag/AlCr-550 (dark red curve) and Ag/AlCr-1300 (pink curve), and (C) Al-1300 tests with three-hour-long isothermal segments (orange curves) and six-hour-long isothermal segments (blue curves); Fig. S6: SEM images of alumina calcined at: (A) 550 °C, (B) 700 °C, (C) 900 °C, (D) 1000 °C, (E) 1100 °C, (F) 1200 °C and (G) 1300 °C; Fig. S7: CO_2 TPD results: Influence of (A) silver deposition and (B) alumina calcination temperature on the CO_2 TPD profile; Fig. S8: Pyridine desorption FTIR measurement results: (A) full spectra of selected supports prior to pyridine adsorption and the 1400–1500 cm^{-1} regions after desorption of pyridine: (B) from selected supports at room temperature, and at different temperatures from (C) Al-550, (D) Al-1300, (E) AlCo-550 and (F) AlCe-1300; the wavenumbers of the minima are given in the graphs; Fig. S9: XRD analysis results: (A) diffraction patterns of the supports calcined at 550 °C, and (B) Ag/Al-550 and Ag/AlCr-550; Fig. S10: XPS results: comparison of survey spectra of (A) AlCr-550, (B) AlCo-550, (C) AlCe-550 and (D) Ag/AlCe-550; Fig. S11: XRD analysis results: (A) diffraction patterns of AlCr-1000, and (B) the supports calcined at 1300 °C; Table S1. Hammett indicator test results of the doped-alumina supports calcined above 550 °C. See DOI: https://doi.org/10.1039/d5ta05994a.

Acknowledgements

This research was funded by the Scientific Discipline Board (RDN) for Chemical Engineering of the Warsaw University of Technology, grant number: 2024 I-CHEM.5-1.3. The authors would like to thank Zbigniew Kaszkur, Polish Academy of Sciences, for performing the XRD measurements, Peter Brodersen, Ontario Centre for the Characterization of Advanced Materials (OCCAM), University of Toronto, for performing the XPS measurements, and Marek Gliński, Warsaw University of Technology, for granting guidance and access to reagents for Hammett indicator tests conducted as part of this study.

References

1 E. Aneggi, J. Llorca, C. de Leitenburg, G. Dolcetti and A. Trovarelli, Soot combustion over silver-supported catalysts, *Appl. Catal., B*, 2009, **91**, 489–498.
2 K. Shimizu, H. Kawachi and A. Satsuma, Study of active sites and mechanism for soot oxidation by silver-loaded ceria catalyst, *Appl. Catal., B*, 2010, **96**, 169–175.
3 L. Nossova, G. Caravaggio, M. Couillard and S. Natis, Effect of preparation method on the performance of silver-zirconia catalysts for soot oxidation in diesel engine exhaust, *Appl. Catal., B*, 2018, **225**, 538–549.
4 M. Montaña, M. S. Leguizamón Aparicio, M. A. Ocsachoque, M. B. Navas, I. de C. L. Barros, E. Rodriguez-Castellón, M. L. Casella and I. D. Lick, Zirconia-Supported Silver Nanoparticles for the Catalytic Combustion of Pollutants Originating from Mobile Sources, *Catalysts*, 2019, **9**, 297.
5 P. Promhuad, B. Sawatmongkhon, K. Theinnoi, T. Wongchang, N. Chollacoop, E. Sukjit, S. Tunmee and A. Tsolakis, Effect of Metal Oxides (CeO_2, ZnO, TiO_2, and Al_2O_3) as the Support for Silver-Supported Catalysts on the

Catalytic Oxidation of Diesel Particulate Matter, *ACS Omega*, 2024, **9**, 19282–19294.

6 Z. Zhao, J. Ma, M. Li, W. Liu, X. Wu and S. Liu, Model Ag/CeO_2 catalysts for soot combustion: Roles of silver species and catalyst stability, *Chem. Eng. J.*, 2022, **430**, 132802.

7 N. Bogdanchikova, F. C. Meunier, M. Avalos-Borja, J. P. Breen and A. Pestryakov, On the nature of the silver phases of Ag/Al_2O_3 catalysts for reactions involving nitric oxide, *Appl. Catal., B*, 2002, **36**, 287–297.

8 X. She and M. Flytzani-Stephanopoulos, The role of Ag–O–Al species in silver–alumina catalysts for the selective catalytic reduction of NO_x with methane, *J. Catal.*, 2006, **237**, 79–93.

9 E. M. Iwanek (nee Wilczkowska), D. W. Kirk and Z. Kaszkur, Anomalous behaviour of silver catalyst for soot oxidation explained: state of silver when operating and the influence of potassium ions, *Catal. Sci. Technol.*, 2023, **13**, 6910–6920.

10 M. V. Grabchenko, G. V. Mamontov, V. I. Zaikovskii, V. La Parola, L. F. Liotta and O. V. Vodyankina, The Role of Metal–Support Interaction in Ag/CeO2 Catalysts for CO and Soot Oxidation, *Appl. Catal., B*, 2020, **260**, 118148.

11 D. Chen, Z. Qua, S. Shen, X. Li, Y. Shi, Y. Wang, Q. Fu and J. Wu, Comparative studies of silver based catalysts supported on different supports for the oxidation of formaldehyde, *Catal. Today*, 2011, **175**, 338–345.

12 M. Richter, U. Bentrup, R. Eckelt, M. Schneider, M.-M. Pohl and R. Fricke, The effect of hydrogen on the selective catalytic reduction of NO in excess oxygen over Ag/Al_2O_3, *Appl. Catal., B*, 2004, **51**, 261–274.

13 L. Zeng, L. Cui, C. Wang, W. Guo and C. Gong, Ag-Assisted CeO_2 Catalyst for Soot Oxidation, *Front. Mater. Sci.*, 2019, **13**, 288–295.

14 J. H. Lee, S. H. Lee, J. W. Choung, C. H. Kim and K.-Y. Lee, Ag-incorporated macroporous CeO_2 catalysts for soot oxidation: Effects of Ag amount on the generation of active oxygen species, *Appl. Catal., B*, 2019, **246**, 356–366.

15 J. Grams, A. Ura and W. Kwapiński, ToF-SIMS as a versatile tool to study the surface properties of silica supported cobalt catalyst for Fischer–Tropsch synthesis, *Fuel*, 2014, **122**, 301–309.

16 J. Rogowski, TOF-SIMS study of morphology and chemical composition of wustite-based precursor and iron catalyst for ammonia synthesis, *Appl. Surf. Sci.*, 2019, **469**, 82–89.

17 L.-T. Weng, Advances in the surface characterization of heterogeneous catalysts using ToF-SIMS, *Appl. Catal., A*, 2014, **474**, 203–210.

18 J. Hofmann, M. Rohnke and B. M. Weckhuysen, Recent advances in secondary ion mass spectrometry of solid acid catalysts: large zeolite crystals under bombardment, *Phys. Chem. Chem. Phys.*, 2014, **16**, 5465–5474.

19 E. M. Iwanek (nee Wilczkowska), L. F. Liotta, G. Pantaleo, L. Hu, S. Williams, D. W. Kirk and Z. Kaszkur, Active Probing of a RuO_2/CZ Catalyst Surface as a Tool for Bridging the Gap Between CO Oxidation Catalytic Tests in a Model and Realistic Exhaust Gas Stream, *ACS Mater. Au*, 2024, **4**, 643–653.

20 E. M. Iwanek, A. Goździk and Z. Kaszkur, Investigating the Ag–Support Interaction in Silver Catalysts for Soot Combustion: The Importance of Coordination of Al^{3+} Ions in the Support, *Reactions*, 2025, **6**, 27.

21 A. Priebe, T. Xie, G. Bürki, L. Petho and J. Michler, The matrix effect in TOF-SIMS analysis of two-element inorganic thin films, *J. Anal. At. Spectrom.*, 2020, **35**, 1156–1166.

22 R. N. S. Sodhi, Time-of-flight secondary ion mass spectrometry (TOF-SIMS): versatility in chemical and imaging surface analysis, *Analyst*, 2004, **129**, 483–487.

23 M. P. Seah and A. G. Shard, The matrix effect in secondary ion mass spectrometry, *Appl. Surf. Sci.*, 2018, **439**, 605–611.

24 Q. Bao, T. Bu, J. Yan, C. Zhang, C. Ning, Y. Zhang, M. Hao, W. Zhang and Z. Wang, Synthesis of Methyl Acrylate by Aldol Condensation of Methyl Acetate with Formaldehyde Over Al_2O_3-Supported Barium Catalyst, *Catal. Lett.*, 2017, **147**, 1540–1550.

25 N. T. Tran, P. S. Kumar, Q. Van Le, N. Van Cuong, P. T. T. Phuong, A. A. Jalil, G. Sharma, A. Kumar, A. Sharma, B. V. Ayodele, S. Z. Abidin and D.-V. N. Vo, CO_2 Reforming of CH_4 on Mesoporous Alumina-Supported Cobalt Catalyst: Optimization of Lanthana Promoter Loading, *Top. Catal.*, 2021, **64**, 1–3.

26 S. B. Alreshaidan, A. A. Ibrahim, A. H. Fakeeha, A. M. Almutlaq, F. A. A. Ali and A. S. Al-Fatesh, Effect of Modified Alumina Support on the Performance of Ni-Based Catalysts for CO_2 Reforming of Methane, *Catalysts*, 2022, **12**, 1066.

27 H. Ruan, M. Nishibori, T. Uchiyama, K. Ninomiya, K. Kamitani, K. Kato, Y. Konishi, A. Haensch, N. Barsan, U. Weimard and K. Shimanoe, Soot oxidation performance with a HZSM-5 supported Ag nanoparticles catalyst and the characterization of Ag species, *RSC Adv.*, 2017, **7**, 43789–43797.

28 A. Ausavasukhi, S. Suwannaran, J. Limtrakul and T. Sooknoi, Reversible interconversion behavior of Ag species in AgHZSM-5: XRD, ^{1}H MAS NMR, TPR, TPHE, and catalytic studies, *Appl. Catal., A*, 2008, **345**, 89–96.

29 T. Baba, H. Sawada, T. Takahashi and M. Abe, Chemisorption study of hydrogen and methane by MAS NMR and conversion of methane in the presence of ethylene on Ag-Y zeolite, *Appl. Catal., A*, 2002, **231**, 55–63.

30 S. Akdemir, E. Ozel and E. Suvaci, Solubility of blue $CoAl_2O_4$ ceramic pigments in water and diethylene glycol media, *Ceram. Int.*, 2011, **37**, 863–870.

31 W. Zhang, J. Li, F. Zhong, G. Wu, H. Jiang, W. Zhang and Q. Liu, Preparation and characterization of supercritical fluid–fried ($CoAl_2O_4$) cobalt blue nano-pigment, *J. Asian Ceram. Soc.*, 2021, **10**, 33–39.

32 S. Yuan, Z. Yuanlin, T. Yufei and J. Yangfeng, Fabrication and Coloration Mechanism of $CoAl_2O_4$ Ceramic Pigment by Co precipitation Method, *J. Synth. Cryst.*, 2017, **46**, 79–84.

33 W. Zhang, Z. Li, G. Wu, W. Wu, H. Zeng, H. Jiang, W. Zhang, R. Wu and Q. Xue, Effects of Coloration of Spinel $CoAl_2O_4$ Cobalt Blue Pigments: Composition, Structure, and Cation Distribution, *Inorganics*, 2023, **11**, 368.

34 D. K. Nguyen, Q.-V. Bach, B. Kim, H. Lee, C. Kang and I.-T. Kim, Synthesis of Cr-doped Al_2O_3 by Pechini sol-gel

method and its application for reversible thermochromic sensors, *Mater. Chem. Phys.*, 2019, **223**, 708–714.

35 Z. K. Heiba, M. B. Mohamed and A. M. Wahba, Structural, optical, mechanical, and electronic properties of Cr-doped alumina, *J. Mater. Sci.:Mater. Electron.*, 2020, **31**, 14645–14657.

36 S. Kakooei, J. Rouhi, E. Mohammadpour, M. Alimanesh and A. Dehzangi, Synthesis and Characterization of Cr-Doped Al_2O_3 Nanoparticles Prepared *Via* Aqueous Combustion Method, *Casp. J. Appl. Sci. Res.*, 2012, **1**, 16–22.

37 D. Kundu, T. Manna and G. De, Preparation and Characterization of Thin Optically Transparent Alumina and Ce-doped Alumina, *J. Sol-Gel Sci. Technol.*, 2002, **23**, 145–150.

38 H. Perez-Pastenes, A. Ochoa-Tapia and T. Viveros, Ascencion Montoya Influence of the Synthesis Method on the Properties of Ceria-Doped Alumina, *J. Sol-Gel Sci. Technol.*, 2006, **37**, 49–56.

39 M. Farahmandjou and S. Motaghi, Sol–gel synthesis of Ce-doped α-Al_2O_3: Study of crystal and optoelectronic properties, *Opt. Commun.*, 2019, **441**, 1–7.

40 S. Zhou, Y. Zhou, J. Shi, Y. Zhang, X. Sheng and Z. Zhang, Synthesis of Ce-doped mesoporous c-alumina with enhanced catalytic performance for propane dehydrogenation, *J. Mater. Sci.*, 2015, **50**, 3984–3993.

41 Z.-M. Wang, M. Yamaguchi, I. Goto and M. Kumagai, Characterization of Ag/Al_2O_3 de-NO_x catalysts by probing surface acidity and basicity of the supporting substrate, *Phys. Chem. Chem. Phys.*, 2000, **2**, 3007–3015.

42 M. Z. Hossain, M. B. I. Chowdhury and P. A. Charpentier, Effect of surface acidity of Al_2O_3 supported metal catalysts on catalytic activity and carbon deposition during SCWG of glucose, *Biomass Bioenergy*, 2019, **124**, 142–150.

43 F. Wang, J. Ma, G. He, M. Chen, C. Zhang and H. He, Nanosize Effect of Al_2O_3 in Ag/Al_2O_3 Catalyst for the Selective Catalytic Oxidation of Ammonia, *ACS Catal.*, 2018, **8**, 2670–2682.

44 C. Wang, S. Li, X. Mao, S. Caratzoulas and R. J. Gorte, H-D Exchange of Simple Aromatics as a Measure of Brønsted-Acid Site Strengths in Solids, *Catal. Lett.*, 2018, **148**, 3548–3556.

45 R. J. Gorte, Temperature-programmed desorption for the characterisation of oxide catalysts, *Catal. Today*, 1996, **28**, 405–414.

46 R. J. Gorte, What do we know about the acidity of solid acids?, *Catal. Lett.*, 1999, **62**, 1–13.

47 Y. Zhu, Z. Chen, H. Li, Q. Wang, X. Liu, Y. Hu, C. Su, R. Duan, S. Chen and L. Lan, Effect of oxygen vacancy and highly dispersed MnO_x on soot combustion in cerium manganese catalyst, *Sci. Rep.*, 2023, **13**, 3386.

48 H. Huang, X. Zhang, J. Liu and S. Ye, Study on oxidation activity of Ce-Mn-K composite oxides on diesel soot, *Sci. Rep.*, 2020, **10**, 10025.

49 Q. Liang, X. Wu, D. Weng and H. Xu, Oxygen activation on Cu/Mn–Ce mixed oxides and the role in diesel soot oxidation, *Catal. Today*, 2008, **139**, 113–118.

50 E. García-Bordejé, A. Belén Dongil, J. M. Conesa, A. Guerrero-Ruiz and I. Rodríguez-Ramos, Promotion of Ru or Ni on Alumina Catalysts with a Basic Metal for CO_2 Hydrogenation: Effect of the Type of Metal (Na, K, Ba), *Nanomat*, 2022, **12**, 1052.

51 X. Zhu, X. Hu, X. Wu, Y. Cai, H. Zhang and X. Tu, Ammonia synthesis over γ-Al_2O_3 pellets in a packed-bed dielectric barrier discharge reactor, *J. Phys. D: Appl. Phys.*, 2020, **53**, 164002.

52 P. Mariani, X. Sun, S. Mascotto, L. Raimondo, A. Sassella, D. Monticelli, E. Berretti, A. Lavacchi, M. Stredansky, C. Cepek, S. Mostoni, C. Santoro, B. Di Credico, R. Scotti and M. D'Arienzo, Critical assessment of the exsolution process in Cu-doped $SrTiO_3$ by a combined spectroscopic approach, *Inorg. Chem. Front.*, 2025, **12**, 311–327.

53 H. He, L. Xueting, L. Shujun, W. Zeng, G. Jingheng, W. Junliang, W. Wen, Y. Daiqi and M. Fu, The key surface species and oxygen vacancies in MnO_x(0.4)-CeO_2 toward repeated soot oxidation, *Appl. Catal., B*, 2018, **223**, 134–142.

54 J. Yang, S. Hu, Y. Fang, S. Hoang, L. Li, W. Yang, Z. Liang, J. Wu, J. Hu, W. Xiao, C. Pan, Z. Luo, J. Ding, L. Zhang and Y. Guo, Oxygen Vacancy Promoted O_2 Activation over Perovskite Oxide for Low-Temperature CO Oxidation, *ACS Catal.*, 2019, **9**, 9751–9763.

55 M. Gliński, D. Armusiewicz, K. Łukasik-Kwaśniewska, M. Materowski, A. Rułka, E. M. Iwanek and M. Kucharska, Diastereoselective Transfer Hydrogenation of Cyclic and Bicyclic Ketones over Selected Metal Oxides as Catalysts, *Molecules*, 2025, **30**, 2153.

56 M. Yurdakoç, M. Akçay, Y. Tonbul and K. Yurdakoç, Acidity of Silica-Alumina Catalysts by Amine Titration Using Hammett Indicators and FT-IR Study of Pyridine Adsorption, *Turk. J. Chem.*, 1999, **23**, 11.

57 E. G. Derouane, J. C. Védrine, R. Ramos Pinto, P. M. Borges, L. Costa, M. A. Lemos, F. Lemos and F. Ramôa Ribeiro, The Acidity of Zeolites: Concepts, Measurements and Relation to Catalysis: A Review on Experimental and Theoretical Methods for the Study of Zeolite Acidity, *Catal. Rev.:Sci. Eng.*, 2013, **55**, 454–515.

58 W. Chen, X. Yi, L. Huang, W. Liu, G. Li, D. Acharya, X. Sun and A. Zheng, Can Hammett indicators accurately measure the acidity of zeolite catalysts with confined space? Insights into the mechanism of coloration, *Catal. Sci. Technol.*, 2019, **9**, 5045–5057.

59 X. Wang, M. He, P. Wang, J. Yao, J. Xiong, X. Zhang, X. Sun, Y. Wei and Z. Li, Alkali metal-enhanced cerium manganese-based three-dimensional ordered macroporous catalyst for NO oxidation and soot combustion, *J. Mater. Chem. A*, 2024, **12**, 24947–24954.

60 C. Qu, P. Wang, M. He, C. Yang, J. Xiong, X. Sun, Y. Wei and Z. Li, Three-dimensional ordered macroporous cerium–manganese composite oxide for NO oxidation, *Catal. Sci. Technol.*, 2023, **13**, 5989–5997.

61 A. H. Fakeeha, Y. A. Al-Baqmaa, A. A. Ibrahim, F. S. Almubaddel, M. F. Alotibi, A. Bentalib, A. E. Abasaeed, A. A. Al-Zahrani, Y. A. Mohammed and A. S. Al-Fatesh, Fe-Promoted Alumina-Supported Ni

Catalyst Stabilized by Zirconia for Methane Dry Reforming, *Catalysts*, 2023, **13**, 806.

62 M. Zarezadeh-Mehrizi, A. Afshar Ebrahimi and A. Rahimi, Comparison of γ and δ-Al_2O_3 supported CoMo catalysts in the hydrodesulfurization of straight-run gas oil, *Sci. Iran.*, 2019, **26**, 1555–1565.

63 M. Gomez, J. Pizarro, X. Castillo, C. Díaz, A. Ghisolfi, M. de Lourdes Chavez, D. Cazorla-Amoros and J. Arenas-Alatorre, Preparation of mesoporous γ-Al_2O_3 with high surface area from an AlOOH extract of recycling biomass ash, *J. Environ. Chem. Eng.*, 2021, **9**, 105925.

64 E. A. Bekele, H. A. Korsa and Y. M. Desalegn, Electrolytic synthesis of γ-Al_2O_3 nanoparticle from aluminum scrap for enhanced methylene blue adsorption: experimental and RSM modeling, *Sci. Rep.*, 2024, **14**, 16957.

65 Y. Huang, X. Peng and X.-Q. Chen, The mechanism of θ- to α-Al_2O_3 phase transformation, *J. Alloys Compd.*, 2021, **863**, 158666.